MNRAS **000**, 000–000 (0000) Preprint 17 August 2018 Compiled using MNRAS LATEX style file v3.0

Near and Mid-infrared properties of known $z \geq 5$ Quasars

Nicholas P. Ross[1]⋆ and Nicholas J. G. Cross[1]
[1]*Institute for Astronomy, University of Edinburgh, Royal Observatory, Edinburgh, EH9 3HJ, United Kingdom*

17 August 2018

ABSTRACT
In this paper, we, for the first time since the discovery of $z \geq 5$ quasars, assemble all spectroscopically confirmed very high redshift quasars in one catalogue. In particular we present the near ($zZyYJHK_s$ and K) infrared and mid-infrared (WISE) properties of all 424 spectroscopically confirmed redshift $z \geq 5.00$ quasars. Using archival public WFCAM/UKIRT and VIRCAM/VISTA data we check for photometric variability in the near-infrared that might be expected from Super-Eddington accretion and find *blah*. We present a comprehensive series of colour-redshift and colour-colour plots and make inferences into the hot dust properties of the very high-redshift quasar population. Extrapolating the known quasar luminosity function we suggest that x% of the possibly detected $z \geq 5$ quasars in the current datasets have been discovered.

Key words: Astronomical data bases: surveys – Quasars: general – galaxies: evolution – galaxies: infrared.

1 INTRODUCTION

Very high redshift quasars (VHzQ; defined here to have redshifts $z \geq 5.00$) are excellent probes of the early Universe. This includes studies of the Epoch of Reionization for hydrogen (see e.g. Fan et al. 2006; Mortlock 2016, for reviews), the formation and build-up of supermassive black holes (e.g., Rees 1984; Wyithe & Loeb 2003; Volonteri 2010; Agarwal et al. 2016; Valiante et al. 2018; Latif et al. 2018) and early metal enrichment (see e.g., Simcoe et al. 2012; Chen et al. 2017; Bosman et al. 2017).

Super-Eddington (also called super-critical) accretion is a viable physical mechanism to explain the high luminosity and rapid growth of supermassive black holes in the early universe (e.g., Alexander & Natarajan 2014; Madau et al. 2014; Volonteri et al. 2015; Pezzulli et al. 2016; Lupi et al. 2016; Pezzulli et al. 2017; Takeo et al. 2018). Thus, one might well expect VHzQs to vary in luminosity as they potentially go through phases of Super-Eddington accretion and these signatures of photometric variablity should be looked for, especially when the e.g. near-infrared K-band is sampling rest-frame ≈3670, 3145, 2750Å at redshifts $z = 5, 6$ and 7, respectively.

Quasars are also known to be prodigious emitters of infrared emission, thought to be from the thermal emission of dust grains heated by continuum emission from the accretion disc (e.g., Richards et al. 2006; Leipski et al. 2014; Hill et al. 2014; Hickox et al. 2017). Observations in the mid-infrared, e.g. ∼3-30μm allow discrimination between AGN[1] and passive galaxies due to the 1.6μm "bump" entering the MIR at $z \approx 0.8 - 0.9$ (e.g., Wright et al. 1994; Sawicki 2002; Lacy et al. 2004; Stern et al. 2005; Richards et al. 2006; Timlin et al. 2016) as well as AGN and star-forming galaxies due to the presence of Polycyclic Aromatic Hydrocarbon (PAHs) at $\lambda > 3\mu$m (e.g., Yan et al. 2007; Tielens 2008).

Jiang et al. (2006) and Jiang et al. (2010) report on the discovery of a quasar without hot-dust emission in a sample of 21 $z \approx 6$ quasars. Such apparently hot-dust-free quasars have no counterparts at low redshift. Moreover, those authors demonstrate that the hot-dust abundance in the 21 quasars builds up in tandem with the growth of the central black hole.

WISE mapped the sky in 4 passbands, in bands centered at wavelengths of 3.4, 4.6, 12, and 23μm. In total the release all sky "ALLWISE" catalog, contains nearly 750 million detections at high-significance[2]. Assef et al. (2013), Stern et al. (2012). Blain et al. (2013) presented WISE mid-infrared (MIR) detections of 17 (55%) of the then known 31 quasars at $z > 6$. However, Blain et al. (2013) was compiled with the WISE 'All-Sky' data release, as opposed to the superior "AllWISE" catalogs. That sample only examined the

⋆ Corresponding Author: npross@roe.ac.uk

[1] Historically, "quasars" and "Active Galactic Nuclei (AGN)" have described different luminosity/classes of objects, but here we use these terms interchangeably (with a preference for quasar) in recognition of the fact that they both describe accreting supermassive black holes (e.g. Haardt et al. 2016).
[2] wise2.ipac.caltech.edu/docs/release/allwise/expsup/sec2_1.html

31 known $z > 6$ quasars; our sample has 148 objects with redshift $z \geq 6.00$.

Here we update Jiang et al. (2010) and Blain et al. (2013) (along with Table 8 of Bañados et al. 2016). Our motivations are numerous and include: *(i)* establishing the first complete catalogue of $z > 5.00$ quasars since the pioneering work from SDSS; *(ii)* reporting homogenous near-infrared photometry for the quasars; *(iii)* making the first study of NIR variability of the VHzQ population and *(iv)* establishing the photometric properties for upcoming surveys and telescopes, e.g. the Large Synoptic Survey Telescope (LSST) [3], ESA *Euclid*[4] and the *James Webb Space Telescope* (JWST)[5]

This paper can be considered an update of Blain et al. (2013) and also an extension of parts of Bañados et al. (2016), with the latter study reporting WISE W1, W2, W3 and W4 magnitudes for Panoramic Survey Telescope and Rapid Response System 1 (Pan-STARRS1, PS1; Kaiser et al. 2002, 2010), but with no further investigation into the reddest WISE waveband for the VHzQs. Bañados et al. (2016) reports and investigates the W1, W2 and W3 properties of quasars at $z > 5.6$. We chose redshift $z = 5.00$ as our lower redshift limit due to a combination of garnishing a large sample, adequately spanning physical properties (e.g. luminosity, age of the Universe) and to incorporate what knowledge we have gained over the last couple of decades since $z > 5$ quasars were discovered.

This paper is organized as follows. In Section 2, we present the assembled list of the 424 $z \leq 5.00$ VHzQs that we have compiled. We then give a high-level overview of the photometric surveys and datasets we use and present the photometry of the VHzQs. In Section 3 we In Section 4 we and we then note our Conclusions in Section 5.

We make the somewhat unconventional decision to present all our photometry and magnitudes on the AB zero-point system (Oke & Gunn 1983; Fukugita et al. 1996). This includes the near-infrared, as well as the mid-infrared magnitudes. Because of established conventions, we report SDSS *ugriz* magnitudes on the AB zero-point system (Oke & Gunn 1983; Fukugita et al. 1996), while the WISE W1 4 magnitudes are calibrated on the Vega system (Wright et al. 2010). For WISE bands, $m_{\rm AB} = m_{\rm Vega} + m$ where m = (2.699, 3.339, 5.174, 6.66) for W1, W2, W3 and W4, respectively (Cutri et al. 2011; Brown et al. 2014). Brown et al. (2014), in PASA, is the paper about Recalibrating the Wide-field Infrared Survey Explorer (WISE) W4 Filter. We make use of the Explanatory Supplement to the WISE All-Sky Data Release, as well as the WISE AllWISE Data Release Products online. We use a flat ΛCDM cosmology with $H0 = 67.7$ km s−1 Mpc1, $\Omega_{\rm M} = 0.307$, and $\Omega_\Lambda = 0.693$ (Planck Collaboration et al. 2016) in order to be consistent with Bañados et al. (2016).

2 DATA

We assemble our dataset in a relatively straightforwad manner. First we compile the list of all known, spectroscopically confirmed quasars from the literature. Most of these objects are easily identified by their broad Lyα emission line, N v emission and characteristic shape blueward of 1215Å observed. As we shall see, some of the more recently discovered objects are close to the galaxy luminosity function characteristic luminosity M^*, and some have relatively weak or maybe even completely absorbed Lyα (e.g. Figures 7 and 10 in Bañados et al. 2016). We leave aside detailed investigation and discussion into espectral features and line strengths, and take as given the published spectra.

We then obtain optical, near-infrared and mid-infrared photometry for the spectral dataset.

The optical data comes from the Panoramic Survey Telescope and Rapid Response System (Pan-STARRS) survey (Chambers et al. 2016) and the Dark Energy Camera (Flaugher et al. 2015), including the Dark Energy Survey (DES; Flaugher 2005) and the Dark Energy Camera Legacy Survey (Dey et al. 2018, DECaLS).

The near-infrared data comes from the Wide Field Camera (WFCAM) on the United Kingdom Infra-Red Telescope

2.1 Very high redshift quasars

In Table 1 we give the discovery reference for the VHzQs noting that some objects were discovered independently and contemporaneously. The redshifts for the VHzQs generally come from the measurement of broad UV/optical emission lines. Where there are far infra-red emission lines e.g. C ii 158 micron, we report these, but at the level of our current analysis broadline redshifts are sufficient.

Specifically, we use data from: Fan et al. (2000), Fan et al. (2001), Fan et al. (2003), Fan et al. (2004), Mahabal et al. (2005), Cool et al. (2006), Fan et al. (2006), Goto (2006), McGreer et al. (2006), Carilli et al. (2007), Kurk et al. (2007), Stern et al. (2007), Venemans et al. (2007), Willott et al. (2007), Jiang et al. (2008), Wang et al. (2008), Jiang et al. (2009), Kurk et al. (2009), Mortlock et al. (2009), Willott et al. (2009), Carilli et al. (2010), Wang et al. (2010), Willott et al. (2010), Willott et al. (2010), De Rosa et al. (2011), Mortlock et al. (2011), Wang et al. (2011), Zeimann et al. (2011), Morganson et al. (2012), Venemans et al. (2012), McGreer et al. (2013), Venemans et al. (2013), Wang et al. (2013), Willott et al. (2013), Bañados et al. (2014), Calura et al. (2014), Leipski et al. (2014), Bañados et al. (2015), Bañados et al. (2015), Becker et al. (2015), Carnall et al. (2015), Jiang et al. (2015), Kashikawa et al. (2015), Kim et al. (2015), Reed et al. (2015), Venemans et al. (2015b), Venemans et al. (2015a), Willott et al. (2015), Wu et al. (2015), Venemans et al. (2016), Wang et al. (2016), Matsuoka et al. (2016), Wang et al. (2016), Mortlock et al. (2011), McGreer et al. (2013), Venemans et al. (2013), Venemans et al. (2013), Venemans et al. (2015b), Venemans

[3] lsst.org
[4] sci.esa.int/euclid/
[5] jwst.nasa.gov; sci.esa.int/jwst; www.asc-csa.gc.ca/eng/satellites/jwst; jwst.stsci.edu

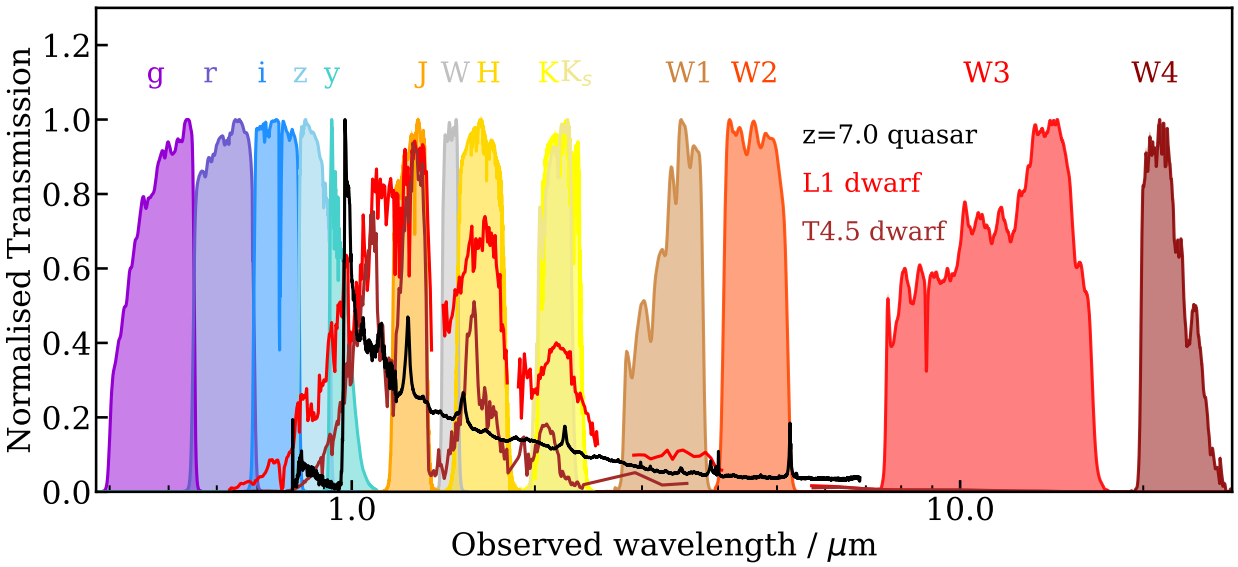

Figure 1. The spectral bands used by different survey telescopes and that are relevant here.

et al. (2015a), Bañados et al. (2016), Matsuoka et al. (2016), Reed et al. (2017), Wang et al. (2017), Mazzucchelli et al. (2017), Ikeda et al. (2017), Tang et al. (2017), Koptelova et al. (2017), Bañados et al. (2018), Matsuoka et al. (2018a) and Matsuoka et al. (2018b).

na	desig	ra_hms	dec_dms	ra	dec	redshift	mag	M1450	w1mag	w1err	w1snr	w2mag	w2err	w2snr	w3mag	w3err	w3snr	v
PSO	J000.3401+26.8358	00:01:21.63	+26:50:09.17	0.34011348	26.83588138	5.75	19.52	-27.16	16.373	0.066	16.5	15.266	0.107	10.2	12.594	0.492	2.2	8
SDSS	J0002+2550	00:02:39.39	+25:50:34.80	0.66411726	25.84304425	5.82	19.39	-27.31	16.162	0.057	19.0	15.542	0.127	8.5	12.416	0.423	2.6	8
SDSS	J0005-0006	00:05:52.34	-00:06:55.80	1.4680833	-0.1154999	5.85	20.98	-25.73	17.299	0.16	6.8	17.043	-9.99	0.2	12.445	-9.99	-1.1	9
PSO	J002.1073-06.4345	00:08:25.77	-06:26:04.60	2.10739	-6.43456	5.93	20.41	-26.32	16.809	0.107	10.1	15.684	0.141	7.7	11.892	-9.99	1.5	8
SDWISE	J0008+3616	00:08:51.43	+36:16:13.49	2.2142917	36.2704138	5.17	19.12	-27.34	16.045	0.052	20.7	15.373	0.092	11.8	12.043	-9.99	1.8	8
PSO	J002.3786+32.8702	00:09:30.89	+32:52:12.94	2.37870183	32.87026179	6.1	21.13	-25.65	-9.99	-9.9	-99.99	-9.99	-9.9	-99.99	-9.99	-9.9	-9.99	-
SDSS	J0017-1000	00:17:14.68	-10:00:55.4	4.3111666	-10.01539722	5.011	99.99	-99.99	15.936	0.055	19.7	15.167	0.094	11.5	12.026	0.334	3.2	8
PSO	J004.3936+17.0862	00:17:34.47	+17:05:10.70	4.39361347	17.08630447	5.8	20.69	-26.01	-9.99	-9.9	-99.99	-9.99	-9.9	-99.99	-9.99	-9.9	-9.99	-
PSO	J004.8140-24.2991	00:19:15.38	-24:17:56.98	4.81408	-24.29916	5.68	19.43	-27.24	16.281	0.069	15.8	15.569	0.116	9.4	12.123	0.344	3.2	8
VDES	J0020-3653	00:20:31.46	-36:53:41.8	5.1311237	-36.8949476	6.9	99.99	-99.99	16.844	0.094	11.6	16.354	0.204	5.3	12.679	-9.99	-0.1	8

Table 1. All 425 $z \geq 5.00$ quasars that have been spectroscopically confirmed as of 2018 June. The first ten objects are given here as guidance to the format of the data table. The full table can be found online.

na	desig	ra_hms	dec_dms	ra	dec	redshift	mag	M1450	w1mag	w1err	w1snr	w2mag	w2err	w2snr	w3mag	w3err	w3snr	v
PSO	J000.3401+26.8358	00:01:21.63	+26:50:09.17	0.34011348	26.83588138	5.75	19.52	-27.16	16.373	0.066	16.5	15.266	0.107	10.2	12.594	0.492	2.2	8
SDSS	J0002+2550	00:02:39.39	+25:50:34.80	0.66411726	25.84304425	5.82	19.39	-27.31	16.162	0.057	19.0	15.542	0.127	8.5	12.416	0.423	2.6	8
SDSS	J0005-0006	00:05:52.34	-00:06:55.80	1.4680833	-0.1154999	5.85	20.98	-25.73	17.299	0.16	6.8	17.043	-9.99	0.2	12.445	-9.99	-1.1	9
PSO	J002.1073-06.4345	00:08:25.77	-06:26:04.60	2.10739	-6.43456	5.93	20.41	-26.32	16.809	0.107	10.1	15.684	0.141	7.7	11.892	-9.99	1.5	8
SDWISE	J0008+3616	00:08:51.43	+36:16:13.49	2.2142917	36.2704138	5.17	19.12	-27.34	16.045	0.052	20.7	15.373	0.092	11.8	12.043	-9.99	1.8	8
PSO	J002.3786+32.8702	00:09:30.89	+32:52:12.94	2.37870183	32.87026179	6.1	21.13	-25.65	-9.99	-9.9	-99.99	-9.99	-9.9	-99.99	-9.99	-9.9	-9.99	-
SDSS	J0017-1000	00:17:14.68	-10:00:55.4	4.3111666	-10.01539722	5.011	99.99	-99.99	15.936	0.055	19.7	15.167	0.094	11.5	12.026	0.334	3.2	8
PSO	J004.3936+17.0862	00:17:34.47	+17:05:10.70	4.39361347	17.08630447	5.8	20.69	-26.01	-9.99	-9.9	-99.99	-9.99	-9.9	-99.99	-9.99	-9.9	-9.99	-
PSO	J004.8140-24.2991	00:19:15.38	-24:17:56.98	4.81408	-24.29916	5.68	19.43	-27.24	16.281	0.069	15.8	15.569	0.116	9.4	12.123	0.344	3.2	8
VDES	J0020-3653	00:20:31.46	-36:53:41.8	5.1311237	-36.8949476	6.9	99.99	-99.99	16.844	0.094	11.6	16.354	0.204	5.3	12.679	-9.99	-0.1	8

Table 2. *This can easily be a second table with e.g. the NIR data...*

Survey	# VHzQs	Notes
ATLAS	4	
CFHQS	20	
DELS	2	
ELAIS	1	
FIRST	1	
HSC	8	
IMS	1	
MMT	12	
NDWFS	1	
PSO	84	
RD	1	
SDSS	156	
SOUV	20	
SDWISE	27	
SHELLQs	55	
ULAS	10	
VDES	11	
VIK	9	
VIMOS	1	

Table 3. ATLAS Shanks et al. (2015);

Table 1 gives the salient details for the objects used in this study. We use all the $z \geq 5.00$ quasars that have been discovered and spectroscopically confirmed as of the time of writing (2018 June). We report near-infrared ($yYJHK$-bands) and mid-infrared (WISE W1/2/3/4) photometry and give our caculcated M_{1450}

2.2 Optical Photometry

2.2.1 Pan-STARRS1 (PS1)

We query the Panoramic Survey Telescope and Rapid Response System (Pan-STARRS)[6] Data Release 1 (DR1) Catalog Archive Server Jobs System (CasJobs) service at mastweb.stsci.edu/ps1casjobs/. The PS1 survey observed the 30,000 deg^2 of sky north of declination -30 degrees in five filters *grizy*. Pan-STARRS1 (PS1) is the first part of Pan-STARRS to be completed and is the basis for the DR1. Chambers et al. (2016), Magnier et al. (2016c), Waters et al. (2016), Magnier et al. (2016a), Magnier et al. (2016b) and Flewelling et al. (2016) describe the instrument, survey, and data analyses. The principal science product of the PS1 survey is the catalog accessible through the CasJobs interface.

We query and return the mean PSF magnitudes from the *grizy* filters (`MeanPSFMag`) which are in the AB system for our 424 VHzQ sample. Details of our SQL and links to the main tables are given in C.

2.2.2 DECam

2.3 Near-infrared photometry

Due to their selection of being very faint/undetected in the observed-frame optical but bright in the observed frame near-infrared, VHzQs are generally detected in the near-infrared $yYJHK$-bands (≈0.98-2.38μm; e.g., Peth et al. 2011).

We query the WFCAM Science Archive (WSA; Hambly et al. 2008) which reports NIR photometry from the Wide Field Camera (WFCAM; Casali et al. 2007) on the United Kingdom Infrared Telescope (UKIRT). Data from the VIRCAM (VISTA InfraRed CAMera) on the VISTA (Visible and Infrared Survey Telescope for Astronomy; Emerson et al. 2006; Dalton et al. 2006) is also given in the WSA.

Quasars are known to vary (both photometrically and spectroscopically) and very high-z quasars under going super-Eddington accretion during a rapid BH growth phase are prime candidates for this variation. Therefore, with repeat observations over many epochs availble via the WSA, we have a choice to make for how we report the photometry. After tests, we decide to give the NIR photometry averaged on 4 week observed timescales. This time bracket is chosen as a good compromise between maximising signal-to-noise while keeping the cadence high. At our observed redshifts, we sample $\lesssim$ 1week in the rest-frame and luminous quasars are not expected to vary on timescales quicker than this (e.g., Lawrence 2016).

We give our recipe and SQL query syntax in Appendix D.

3 NIR DATA

The near-infrared data in this paper comes from the Wide Field Astronomy Unit's (WFAU) Science Archives for UKIRT-WFCAM, the WFCAM Science Archive (WSA Hambly et al. 2008) and VISTA-VIRCAM, the VISTA Science Archive (VSA Cross et al. 2012). These archives were developed for the VISTA Data Flow System (VDFS Emerson et al. 2004).

In this paper we include all non-proprietary WFCAM data, which covers all public surveys and PI projects from Semester 05A to 1st January 2017 and all non-proprietary VISTA data, which covers all public surveys and PI projects from science verification (200910..) to 1st April 2016, to get as much coverage as possible. Hence, the NIR is extremely heterogeneous.

The data was processed using a forced photometry, or matched-aperture photometry. A pipeline for this has been developed by WFAU, but has not yet been incorporated into the main VDFS pipeline. Full details of the matched-aperture pipeline (MAP) will appear in a forthcoming paper, Cross et al. 2018, in prep, and has also been discussed in Cross et al. (2013) and **?**. We will give the pertinent points of the MAP and specific details of these data sets below.

3.1 Selection of NIR

The first step of the process was to ingest the catalogue of VHzQs into the WSA/VSA. These data are in the table `finalQsoCatalogue`. Next we set up new programmes WSERV1000, VSERV1000 in the WSA and VSA respectively. We assign all frames that contain the high-z QSO based on WCS information in the WSA to WSERV1000, but adding a new line to the table `ProgrammeFrame` and same in VSA for VSERV1000. Assigning these frames to a separate programme allows us to process them together and put them into a single release.

[6] https://outerspace.stsci.edu/display/PANSTARRS

3.2 Setup Matched Aperture Product

Add a new entry `RequiredMatchedApertureProduct`

- mapID archiveName programmeID extractor mapType name description selection finalProductTable addSurveyList
- 1 1 WSA 10999 CASU 2 highzQsoMap Variability via matched apertures for set of high-z QSOs SELECTSTR qsoID,ra,dec FROMSTR finalQsoCatalogue highzQsoMap-Variability NONE

Explain
Entries in `RequiredMapAverages`
Add table?

3.3 Processing MAP data

A set of apertureIDs were created in `MapApertureIDshighzQsoMap`, based on the `RequiredMatchedApertureProduct` **selection** value. This may seem unnecessary layer since it is a one-to-one match with `finalQsoCatalogue`, but the layer is a general abstraction that allows multiple sources of catalogue, and multiple types... Entries added to `MapSurveyTables` ⇒ not pertinent

3.3.1 Forced photometry

CASU's `imcore_list` was run on each frame assigned to the programme with the input list equal to objects selected to be within ...of the multiframe centre. In this case, where there are 424 QSOs spread across the sky, there is typically 1 object per multiframe, but many have two and one, multiframeID=2614475 in the VSA, has 3 objects. The output of `imcore_list` is a multi-extension FITS binary table, with identical columns to the CASU FITS binary tables produced using the CASU `imcore`, the basis of all WFCAM and VISTA survey products and also familiar to many astronomers through the INTWFS (), and VST-ATLAS and -VPHAS (). Since forced photometry can be run in many ways on a particular image, a single science frame is not necessarily linked to a single MAP catalogue, so the `MapFrameStatus` table links images (**multiframeID**) to catalogues (**catalogueID**) and gives information on what processing stage they are at (**bitProcessingFlag**), whether they have been ingested (**isIngested**), or what quality control has been run on them (**ppErrBitsStatus**).

For matched aperture measurements, we process these binary tables using the same software, as the standard extracted catalogues, but implement a few different processes. We calculate both Luptitudes (Lupton et al. 1999), and calibrated fluxes, see Eqn 1.

$$F^{calib} = f \times 10^{-0.4*(ZP+VAB-8.90+corr)} \quad (1)$$

where f is the measured flux in ADU, ZP is the zeropoint of frame, VAB is the Vega-to-AB correction for the filter, and $corr$ are the various correction terms, e.g. distortion correction, scattered light correction, aperture correction, see (Hambly et al. 2008; Cross et al. 2012).

Once all data is processed, the data are ingested into `wserv1000MapRemeasurement` and `vserv1000MapRemeasurement` respectively. These tables are similar in structure to `lasDetection` described in (Hambly et al. 2008) or other UKIDSS or VISTA detection tables. One of the main differences is the primary key which is (**apertureID**,**catalogueID**) rather than (**multiframeID**,**extNum**,**seqNum**), reflecting the fact that these are forced photometry on a known set of apertures and a set of catalogues, rather than detections above a threshold in a set of detector extensions to image multiframes.

3.3.2 Averaging matched photometry

Unfortunately the photometry in a single epoch image often has low signal-to-noise. The advantage of matched aperture photometry on QSOs is that co-adding is relatively simple: if each epoch is taken in the same aperture (assuming the astrometry is correct) and the aperture photometry has been corrected to total: the standard aperture corrections work well for point sources then averaging the calibrated photometry should give as good as extracting from a deep stack. In fact it will almost certainly do better, since the images in some cases are taken from multiple projects with different pointings. In addition, corrections such as scattered light, pixel distortion and aperture corrections will be more complex, if not impossible to apply to deep-stacks but will be automatically applied in the averaging of forced photometry.

We average the aperture corrected calibrated fluxes (e.g. **aperJky3**), and then convert to magnitudes or luptitudes. Since we do not have a deep image for each set of averages, we cannot calculate non-aperture corrected values, so the photometry is only appropriate for point-sources.

$$\bar{F} = \frac{\sum_i^N (w_i\, F_i)}{\sum_i^N w_i} \quad (2)$$

where F_i is the i^{th} epoch measurement of a parameter to be averaged such as the aperture corrected calibrated flux in a $1''$ aperture (**aperJky3**) and $\bar{F}$ is the weighted mean average of this parameter. The weight for each epoch $w_i = 1/(\sigma_F)^2$ if the epoch is included and $w_i = 0$ if an epoch is excluded for quality control purposes. We exclude inputs where the bitwise quality flag, **ppErrBits**¿256, and additionally, in the case of VISTA, we exclude data on detector 16 (**extNum=17**), where the quantum efficiency is variable. If all remeasurements are excluded, then one of the ones with the lowest **ppErrBits** is used. In this case the averages will be equal to the original measurement, and the reader may wonder why we bother to duplicate the data. It is important to do this to simplify queries for users who will then not have to set up complex queries to work out where the data is, and only around 2% of VISTA MAP measurements were excluded so the fraction of duplications is very low. The average data is stored in `wserv1000MapRemeasAver` for WFCAM and `vserv1000MapRemeasAver` for VISTA, which again are organised with a primary key of (**apertureID**,**catalogueID**). Some parameters that are averaged do not have an error σ_F, so in these cases we weight them using the **averageConf** parameter, which has a median of 100. In the case of WFCAM where this is not calculated, we set each epoch to have an **averageConf**= 100. The **sumWeights** param-

	programmeID	mapID	setupID	description	useDeeps	useHighProd	timeScale	nEpochs	overLaps
1	10999	1	1	Average over a week	0	NONE	+7.000000	-99999999	0
2	10999	1	2	Average over a fortnight	0	NONE	+14.000000	-99999999	0
3	10999	1	3	Average over a month	0	NONE	+30.000000	-99999999	0
4	10999	1	4	Average over 10 epochs	0	NONE	-9.999995E008	10	0
5	10999	1	5	Average over 6 months	0	NONE	+183.000000	-99999999	0
6	10999	1	6	Average over whole time	0	NONE	-1.000000	-99999999	0

Table 4.

eter in the `MapRemeasAver` tables is the sum of all the **averageConf** values that went into the calculation and the `vserv1000MapAverageWeights` table gives the weights for each epoch, linked to each average for VSERV1000.

We calculate a set of averaged catalogues, for each pointing and filter, based on the requirements in `RequiredMapAverages`, in these cases over time spans of 7, 14, 28, 183 days, over 10 epochs and finally over all epochs. The averaging process starts at the first epoch and works on. Possible future refinements could first look for denser groupings that satisfied the criteria so that these were not split into two groups.

Each averaged catalogue has a separate entry in `MapFrameStatus` and is linked to each original epoch remeasured catalogue through `MapProvenance`, which contains the averaged catalogue identifier **combiCatID**, the epoch catalogue identifier **catalogueID** and the averaging setup ID **avSetupID**.

3.3.3 ...

The code to calculate variability statistics as described in Cross et al. (2009) has not yet been completed to run with the matched aperture pipeline, so these are not included.

3.3.4 UKIDSS LAS

Use:
dr10plus
lasSource table (merged catalogue), nearest object only; radius 2.0”
424 results returned. Of which...

3.3.5 VISTA VHS

Use:
VH5DR5
sourceTable (merged catalogue), nearest object only; radius 2.0”
424 results returned. Of which...

N.B., a few objects will have both UKIDSS LAS and VISTA VHS photometry...

4 RESULTS

Lorem ipsum dolor sit amet, consectetur adipiscing elit. Aliquam porta sodales est, vel cursus risus porta non. Vivamus vel pretium velit. Sed fringilla suscipit felis, nec iaculis lacus convallis ac. Fusce pellentesque condimentum dolor, quis vehicula tortor hendrerit sed. Class aptent taciti sociosqu ad litora torquent per conubia nostra, per inceptos himenaeos. Etiam interdum tristique diam eu blandit. Donec in lacinia libero.

4.1 Detection Rates

4.2 Variability

Sed elit massa, eleifend non sodales a, commodo ut felis. Sed id pretium felis. Vestibulum et turpis vitae quam aliquam convallis. Sed id ligula eu nulla ultrices tempus. Phasellus mattis erat quis metus dignissim malesuada. Nulla tincidunt quam volutpat nibh facilisis euismod. Cras vel auctor neque. Nam quis diam risus.

Nunc semper quam et leo interdum vulputate eu quis magna. Sed nec arcu at orci egestas convallis. Aenean quam velit, aliquam vitae viverra in, elementum vel elit. Nunc suscipit aliquet sapien a suscipit. Cras nulla ipsum, posuere eu fringilla sit amet, dapibus ultricies nulla. Nullam eu augue id purus mollis dignissim sed et libero. Phasellus eget justo sed neque pellentesque egestas nec id arcu. Donec facilisis pulvinar sapien et fringilla. Suspendisse vestibulum rhoncus sapien id laoreet. Morbi et orci vitae tortor imperdiet imperdiet. In hac habitasse platea dictumst. Vivamus vel neque id mi ultrices tristique. Integer quam libero, ornare vel gravida in, feugiat a ante. Nam dapibus, tellus vitae pellentesque cursus, dui nisl egestas augue, non fermentum nisl est nec nisi. Vestibulum nec mi justo, eget dapibus velit.

4.3 Very High-z Quasars Detected in WISE

Blain et al. (2013) Cras in laoreet mauris. Vivamus nec nulla a dui commodo adipiscing. Proin vulputate lectus nec arcu iaculis sit amet auctor ligula ultricies. Phasellus condimentum gravida tincidunt. Phasellus et mauris ac nibh vestibulum vehicula. Morbi et augue id purus gravida sagittis quis in sem. Phasellus quis risus bibendum eros luctus auctor.

4.3.1 Very High-z Quasars Detected in WISE W3 and W4

Proin non tempus velit. Etiam laoreet, enim nec scelerisque dictum, tortor massa tempor enim, id pretium justo quam ac lectus. Maecenas diam nibh, interdum at lobortis sit amet, dignissim et quam. Sed tincidunt faucibus risus, congue tempus nisl consectetur eget. Suspendisse venenatis turpis ut risus aliquam interdum. In at velit sed ligula dictum dignissim ut et dui. Curabitur ac scelerisque purus.

4.4 Colours

Pellentesque vel elit neque, in interdum lacus. Quisque sodales, nunc et luctus convallis, nisl dui luctus dui, at congue urna velit a nisl. Ut sit amet sapien a risus dapibus sagittis. Cras sed ultricies erat. Donec id metus sed urna lacinia convallis vel sed enim. Proin nisi libero, ornare vel bibendum eu, sollicitudin sed leo. Cras tincidunt aliquet ultricies. Cras pretium velit leo, in malesuada enim. Duis sagittis ultricies interdum. Proin sit amet sem nec metus feugiat pharetra.

Figure 2 presents the optical colour-redshift trends for Late Type M/L/T dwarfs and the VHzQs.

Figure 2 presents the near-infrared colour-redshift trends for Late Type M/L/T dwarfs and the VHzQs.

4.5 Consequences of evolution of the $M_{\rm BH} - M_\star$ relation

From a study of 69 *Herschel*-detected broad-line active galactic nuclei, Sun et al. (2015) find there is no evolution in the $M_{\rm BH} - M_\star$ relation from $z \sim 2$ to $z \sim 0$, with the ratio of $\log(M_{\rm BH}/M_\star$ constant at -2.85 across this redshift range. If this ratio holds to $z > 5$, and we assume the $M_{\rm BH}$ for the $z > 6$ measured from the e.g. Mg II line, are generally correct, then the galaxy total stellar mass for the $z > 6$ objects should be...

Yang et al. (2018) calculate the long-term SMBH accretion rate as a function of $M_{\rm star}$ and redshift $[BHAR(M_\star, z)]$ over ranges of $\log(M_{\rm star}/M_\odot) = 9.512$ and $z = 0.44$. Our BHAR(M,z) is constrained by high-quality survey data (GOODS-South, GOODS-North and COSMOS), and by the stellar mass function and the X-ray luminosity function. This BHAR/SFR dependence on $M_\star$ does not support the scenario that SMBH and galaxy growth are in lockstep.

4.6 L-z Plane

Having obtained an as-near-to-homogenous set of photometry as we can, we are now in a position to calculate the Absolute Magnitudes of the VHzQ sample and in particulare the absolute magnitude at rest-frame 1450Å' M_{1450}, which is a key physical quantity and goes directly towards the quasar luminosity function and thus the reionization of hydrogen calculation.

At $z = 5.00$, the rest-frame 1450Å emission is redshifted to 8700Å iobserved, i.e., in the z-band, while at

4.7 SEDs and Dust properties of the VHzQs

There are a range of IR SEDs e.g. Mullaney et al. (2013) etc. etc. etc. However, they are, for our purposes all roughly the same.

5 DISCUSSION AND CONCLUSIONS

In this study, we have, for the first time, ompiled the list of all $z > 5$ spectroscopically confirmed quasars. We have assemble the NIR ($y/Y, J, H, K/K_s$) and MIR (WISE W1/2/3/4) photometry for these objects, given their detection rates and SEDs. We find that:

We can gain a good appreciation for what these missions will discover by collating the datasets we currently have.

- Lorem ipsum dolor sit amet, consectetur adipiscing elit. Aliquam porta sodales est, vel cursus risus porta non. Vivamus vel pretium velit. Sed fringilla suscipit felis, nec iaculis lacus convallis ac.
- Fusce pellentesque condimentum dolor, quis vehicula tortor hendrerit sed. Class aptent taciti sociosqu ad litora torquent per conubia nostra, per inceptos himenaeos. Etiam interdum tristique diam eu blandit. Donec in lacinia libero.
- Sed elit massa, eleifend non sodales a, commodo ut felis. Sed id pretium felis. Vestibulum et turpis vitae quam aliquam convallis. Sed id ligula eu nulla ultrices tempus. Phasellus mattis erat quis metus dignissim malesuada. Nulla tincidunt quam volutpat nibh facilisis euismod. Cras vel auctor neque. Nam quis diam risus.

Nunc lacus nibh, convallis ac lobortis ut, tempus ac lectus. Maecenas eu elit massa. Nulla vel lacus lorem. Proin et lobortis tortor. Phasellus ultrices nisl non enim porttitor dictum. Curabitur nec nunc ac nibh ornare elementum. Nunc ultrices hendrerit ultricies. Aliquam dapibus semper est et gravida. Etiam cursus, massa eget tempor elementum, lectus urna feugiat nisi, eget sagittis.

ACKNOWLEDGEMENTS

NPR acknowledges support from the STFC and the Ernest Rutherford Fellowship scheme.

We thank Bernie Shiao at STScI for help with the Pan-STARRS1 DR1 CasJobs interface.

This paper heavily used TOPCAT (v4.4) (Taylor 2005, 2011).

This research made use of `Astropy`, a community-developed core Python package for Astronomy (Astropy Collaboration et al. 2013; The Astropy Collaboration et al. 2018).

The Pan-STARRS1 Surveys (PS1) and the PS1 public science archive have been made possible through contributions by the Institute for Astronomy, the University of Hawaii, the Pan-STARRS Project Office, the Max-Planck Society and its participating institutes, the Max Planck Institute for Astronomy, Heidelberg and the Max Planck Institute for Extraterrestrial Physics, Garching, The Johns Hopkins University, Durham University, the University of Edinburgh, the Queen's University Belfast, the Harvard-Smithsonian Center for Astrophysics, the Las Cumbres Observatory Global Telescope Network Incorporated, the National Central University of Taiwan, the Space Telescope Science Institute, the National Aeronautics and Space Administration under Grant No. NNX08AR22G issued through the Planetary Science Division of the NASA Science Mission Directorate, the National Science Foundation Grant No. AST-1238877, the University of Maryland, Eotvos Lorand University (ELTE), the Los Alamos National Laboratory, and the Gordon and Betty Moore Foundation.

CasJobs was originally developed by the Johns Hopkins University/ Sloan Digital Sky Survey (JHU/SDSS) team. With their permission, MAST used version 3.5.16 to construct CasJobs-based tools for GALEX, Kepler, the Hubble Source Catalog, and PanSTARRS.

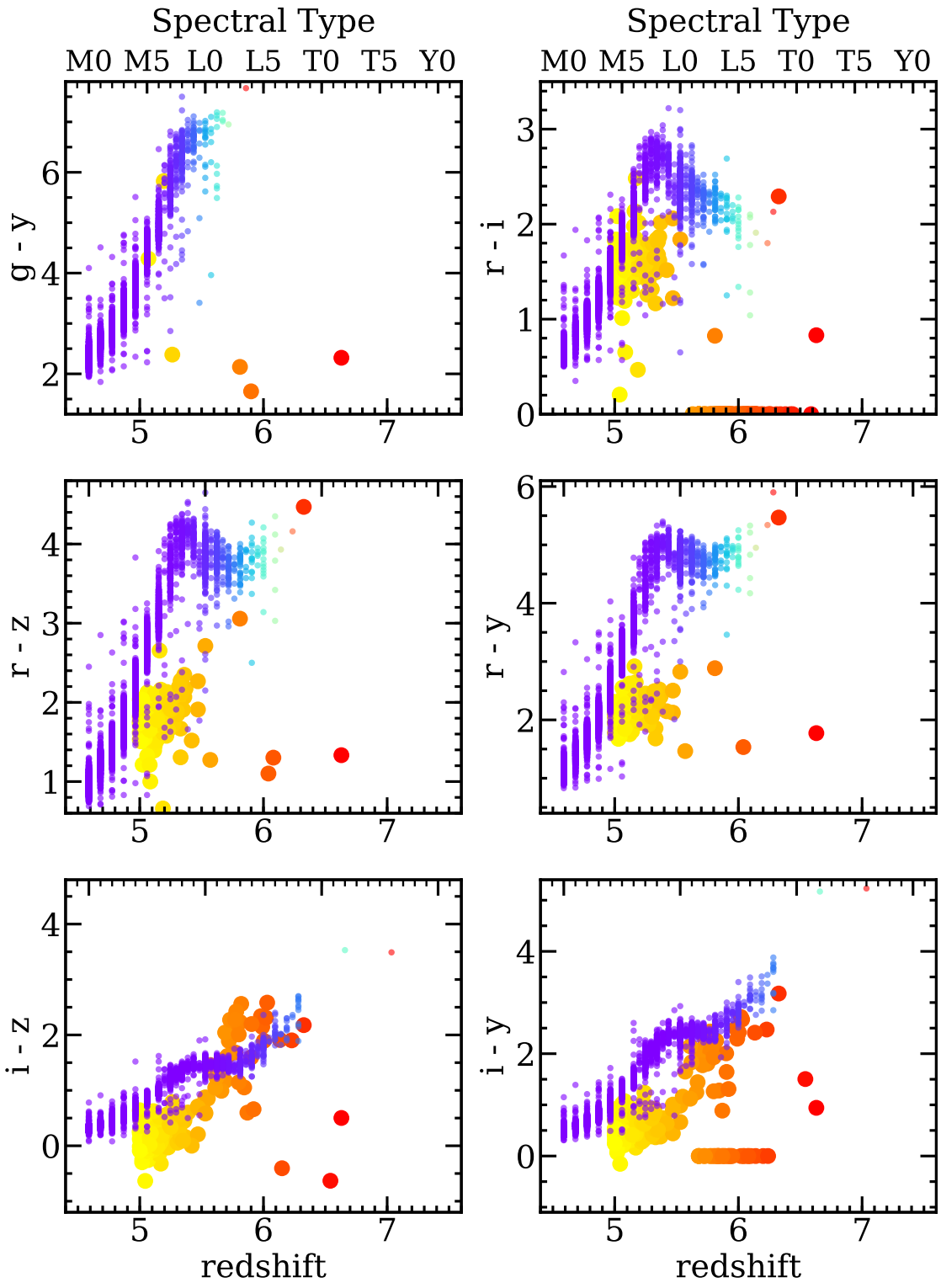

Figure 2. Optical colour vs. spectral type and redshift for Late Type M/L/T dwarfs and the VHzQs. The stars are M, L, and T dwarfs from the Best et al. (2018) PS1-detected catalog. *N.B. Trying to look as good as Fig. 5 from Best et al. (2018). How does one get bigger gaps between subplots??*

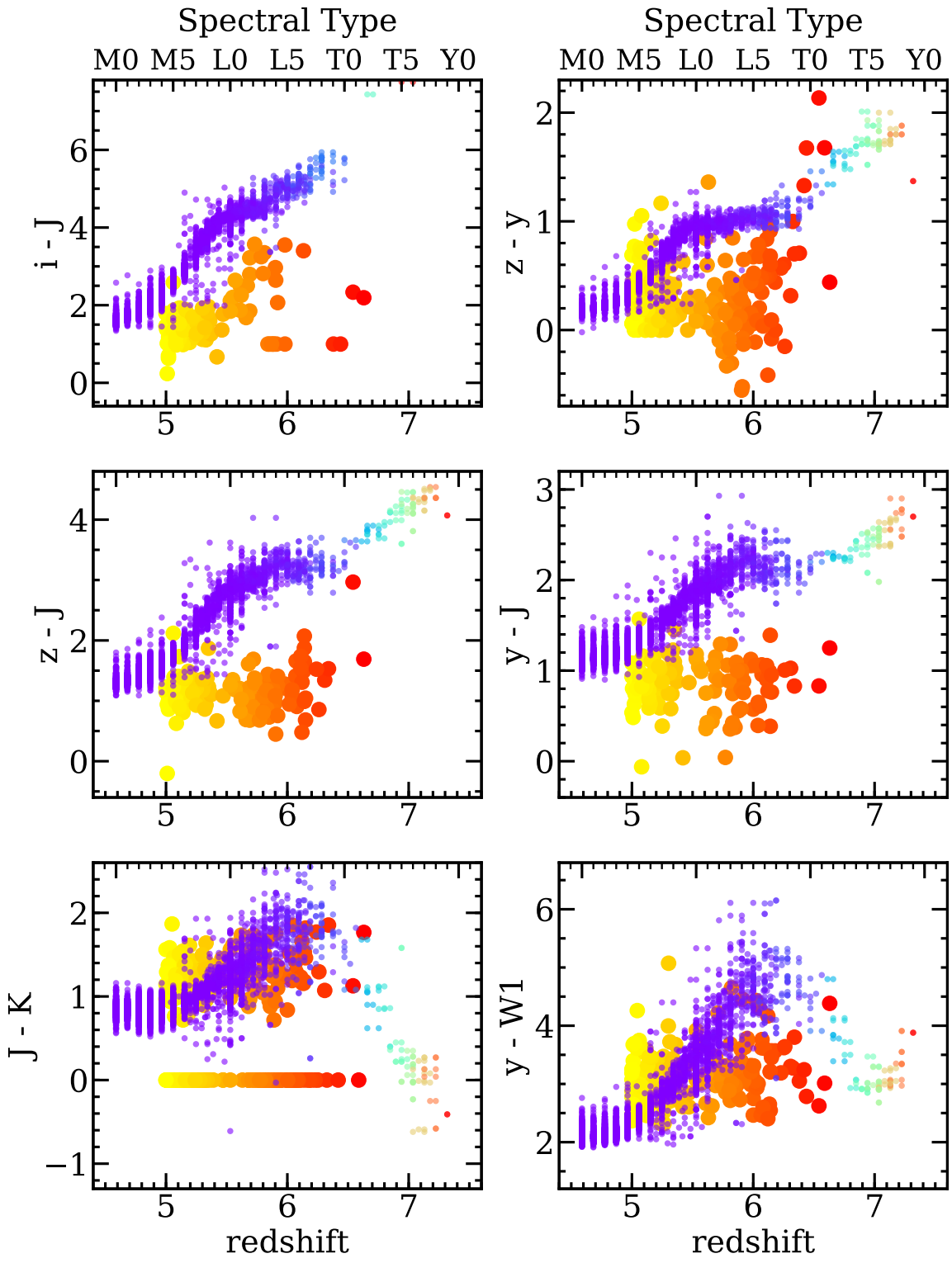

Figure 3. Infrared colour-spectral type and redshift plots for Late Type M/L/T dwarfs and the VHzQs. *NB* I'm really not sure how Best et al. actually get their stellar sequence so clean. There are two types of spectral classification, but restricting it to just SpT_optn or SpT_nir removes the blue or red end respectively. Hmmm....

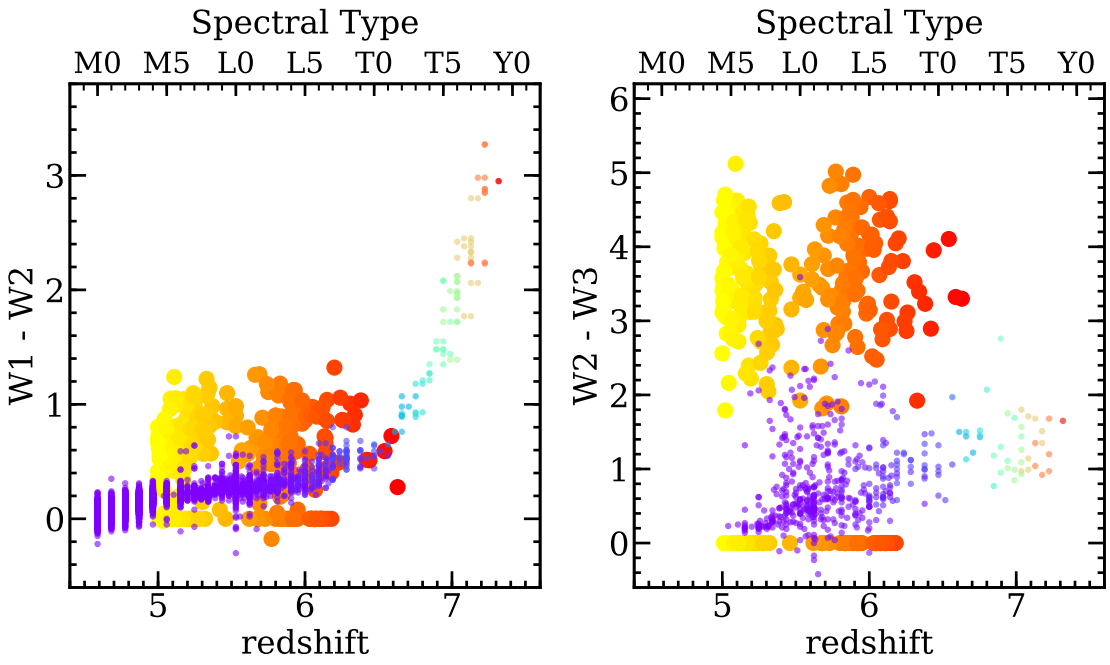

Figure 4. Infrared colour-spectral type and redshift plots for Late Type M/L/T dwarfs and the VHzQs.

This publication makes use of data products from the Wide-field Infrared Survey Explorer, which is a joint project of the University of California, Los Angeles, and the Jet Propulsion Laboratory/California Institute of Technology, and NEOWISE, which is a project of the Jet Propulsion Laboratory/California Institute of Technology. WISE and NEOWISE are funded by the National Aeronautics and Space Administration.

This research has made use of the SVO Filter Profile Service (http://svo2.cab.inta-csic.es/theory/fps/) supported from the Spanish MINECO through grant AyA2014-55216 The SVO Filter Profile Service[7] describes the Spanish VO Filter Profile Service. The Filter Profile Service Access Protocol. Rodrigo, C., Solano, E. http://ivoa.net/documents/Notes/SVOFPSDAL/index.html

APPENDIX A: FILTER CURVES

FRom the SVO Filter Profile Service[8].

APPENDIX B: A. PHOTOMETRIC BANDS AND CONVERSIONS

Due to the differing normalizations between the SDSS and UKIDSS photometric systems, certain corrections are required. To present our data in the purest sense, all the NIR magnitudes from UKIDSS (originally AB magnitudes) were corrected to Vega magnitudes as suggested in Hewett et al. (2006).

Although ULAS magnitudes are reported in terms of Vega and SDSS magnitudes are reported in AB terms for the most part whenever an optical-NIR color was calculated both magnitudes were left in their default term.

https://www.gemini.edu/sciops/instruments/magnitudes-and-fluxes

APPENDIX C: PANSTARRS1 SQL QUERIES

The PS1 Casjobs SQL Server is located at mastweb.stsci.edu/ps1casjobs. The top level documentation is given here while the description of tables is given here. The main tables are the `objectThin` and `meanObject` tables.

[7] Rodrigo, C., Solano, E., Bayo, A. http://ivoa.net/documents/Notes/SVOFPS/index.html

[8] http://svo2.cab.inta-csic.es/svo/theory/fps/

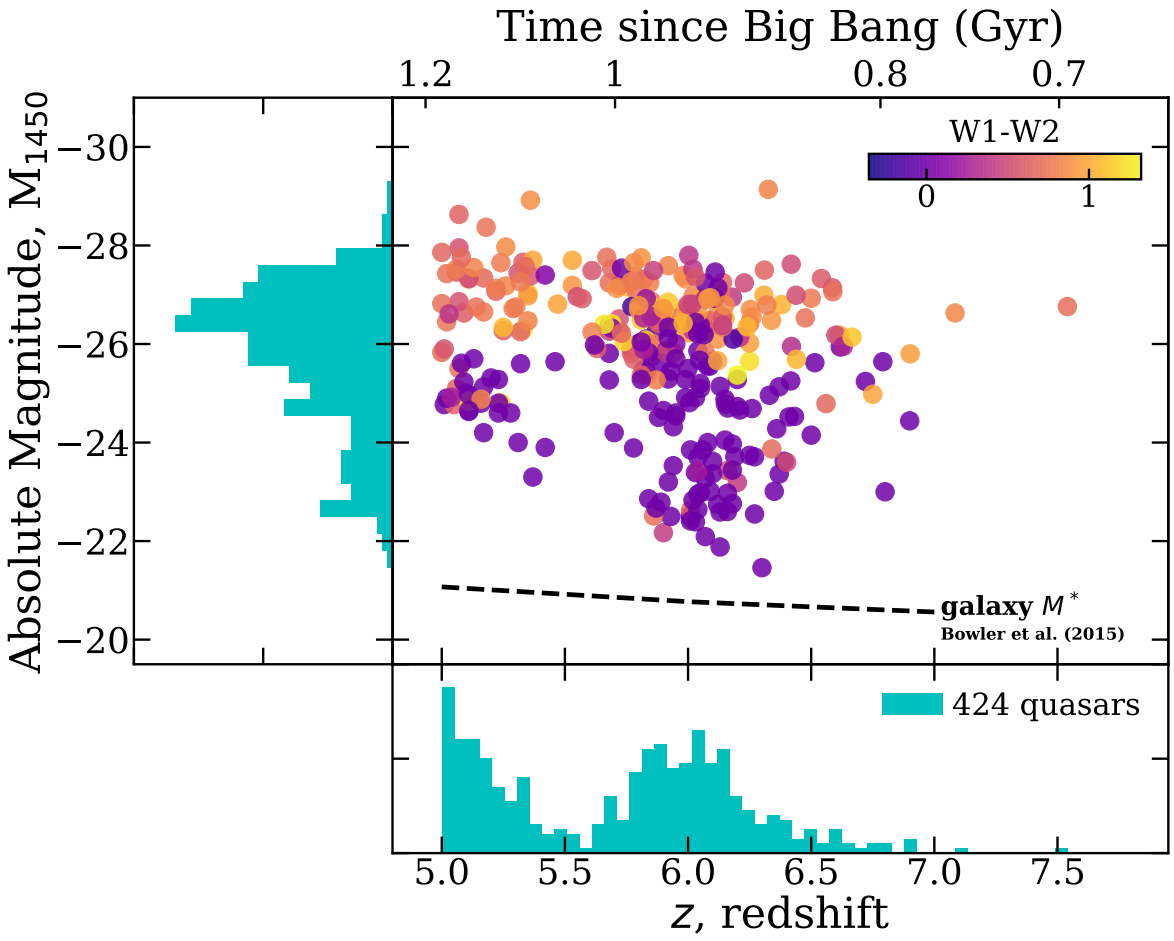

Figure 5. The spectral bands used by different survey telescopes and that are relevant here.

APPENDIX D: NEAR-INFRARED WFCAM SCIENCE ARCHIVE SQL QUERIES

Here we give the receipe and SQL that returned the near-infrared photometry for the VHzQs.

(i) http://wsa.roe.ac.uk/
(ii) Login
(iii) `username: WSERV1000; password: highzqso; community: nonSurvey`
(iv) Freeform SQL Query with WSERV1000v20180327

Then the following SQL will return the values in Table 1.

```
SELECT
qso.qsoName, qso.ra, qso.dec,
aver.apertureID, aver.aperJky3,
aver.aperJky3Err, aver.sumWeight,
aver.ppErrBits, m.mjdObs,
m.filterID, remeas.aperJky3,
remeas.aperJky3Err,
w.weight, remeas.ppErrBits,
m.project

FROM
highzQsoInput as qso,
MapApertureIDshighzQsoMap as ma,
wserv1000MapRemeasAver as aver,
wserv1000MapRemeasurement as remeas,
MapProvenance as v,
wserv1000MapAverageWeights as w,
MapFrameStatus as mfs,
Multiframe as m

WHERE
qso.qsoID=ma.objectID and
ma.apertureID=aver.apertureID and
aver.apertureID=remeas.apertureID and
aver.catalogueID=v.combicatID and
v.avSetupID=1 and
v.catalogueID=remeas.catalogueID and
w.combicatID=v.combicatID and
w.catalogueID=v.catalogueID and
w.apertureID=aver.apertureID and
mfs.catalogueID=remeas.catalogueID and
m.multiframeID=mfs.multiframeID and
```

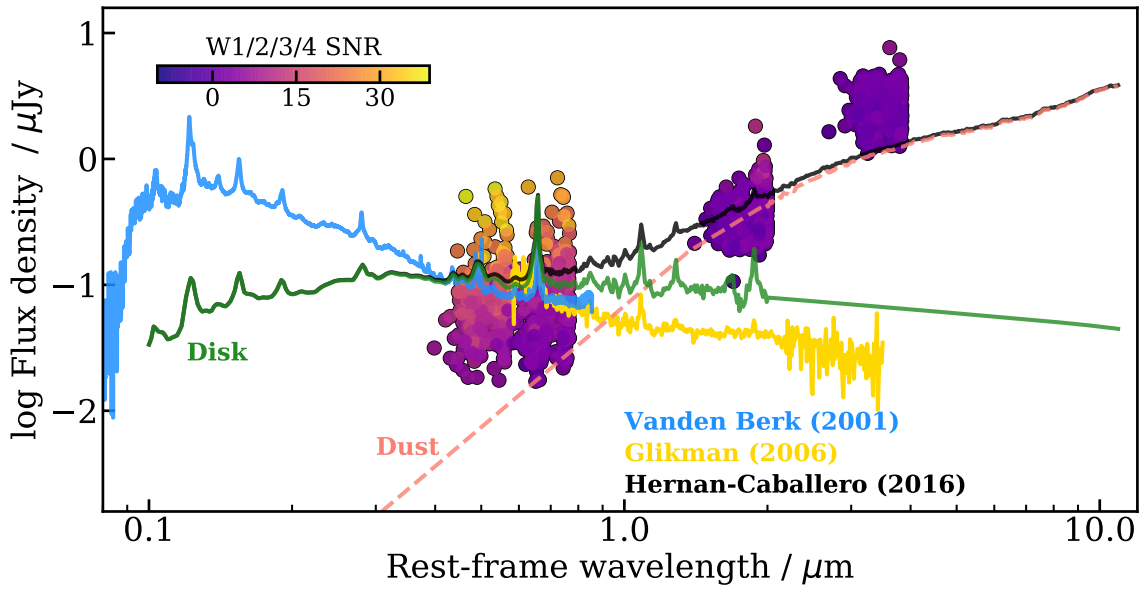

Figure 6. The rest-frame properties of the VHzQs.

```
33 mfs.programmeID=10999 and
34 mfs.mapID=1
35 order by v.combicatID, m.mjdObs
```

REFERENCES

Agarwal B., Smith B., Glover S., Natarajan P., Khochfar S., 2016, MNRAS, 459, 4209

Alexander T., Natarajan P., 2014, Science, 345, 1330

Assef R. J., et al., 2013, ApJ, 772, 26

Astropy Collaboration et al., 2013, Astron. & Astrophys., 558, A33

Bañados E., Decarli R., Walter F., Venemans B. P., Farina E. P., Fan X., 2015, ApJ Lett., 805, L8

Bañados E., et al., 2014, AJ, 148, 14

Bañados E., et al., 2015, ApJ, 804, 118

Bañados E., et al., 2016, ApJS, 227, 11

Bañados E., et al., 2018, Nat, 553, 473

Becker G. D., Bolton J. S., Lidz A., 2015, PASA, 32, 45

Best W. M. J., et al., 2018, ApJS, 234, 1

Blain A., et al., 2013, ArXiv e-prints

Bosman S. E. I., et al., 2017, MNRAS, 470, 1919

Brown M. J. I., Jarrett T. H., Cluver M. E., 2014, PASA, 31, 49

Calura F., Gilli R., Vignali C., Pozzi F., Pipino A., Matteucci F., 2014, MNRAS, 438, 2765

Carilli C. L., et al., 2007, ApJ Lett., 666, L9

Carilli C. L., et al., 2010, ApJ, 714, 834

Carnall A. C., Shanks T., Chehade B., Fumagalli M., Rauch M., Irwin M. J., Gonzalez-Solares E., Findlay J. R., Metcalfe N., 2015, MNRAS, 451, L16

Casali M., et al., 2007, Astron. & Astrophys., 467, 777

Chambers K. C., et al., 2016, arXiv:1612.05560v3

Chen S.-F. S., et al., 2017, ApJ, 850, 188

Cool R. J., et al., 2006, AJ, 132, 823

Cross N., Hambly N., Collins R., Sutorius E., Read M., Blake R., 2013, in Adamson A., Davies J., Robson I., eds, Thirty Years of Astronomical Discovery with UKIRT Vol. 37 of Astrophysics and Space Science Proceedings, Discovery of Variables in WFCAM and VISTA Data. p. 193

Cross N. J. G., Collins R. S., Hambly N. C., Blake R. P., Read M. A., Sutorius E. T. W., Mann R. G., Williams P. M., 2009, MNRAS, 399, 1730

Cross N. J. G., Collins R. S., Mann R. G., Read M. A., Sutorius E. T. W., Blake R. P., Holliman M., Hambly N. C., Emerson J. P., Lawrence A., Noddle K. T., 2012, Astron. & Astrophys., 548, A119

Cross N. J. G., et al., 2012, Astron. & Astrophys., 548, A119

Cutri R. M., et al., 2011, Technical report, Explanatory Supplement to the WISE Preliminary Data Release Products

Dalton G. B., et al., 2006, in Society of Photo-Optical Instrumentation Engineers (SPIE) Conference Series Vol. 6269 of Proc. SPIE, The VISTA infrared camera. p. 62690X

De Rosa G., Decarli R., Walter F., Fan X., Jiang L., Kurk J., Pasquali A., Rix H. W., 2011, ApJ, 739, 56

Dey A., et al., 2018, ArXiv e-prints

Emerson J., McPherson A., Sutherland W., 2006, The Messenger, 126, 41

Emerson J. P., Irwin M. J., Lewis J., Hodgkin S., Evans D., Bunclark P., McMahon R., Hambly N. C., Mann R. G., Bond I., Sutorius E., Read M., Williams P., Lawrence A., Stewart M., 2004, in P. J. Quinn & A. Bridger ed., Society of Photo-Optical Instrumentation Engineers (SPIE) Conference Series Vol. 5493 of Society of Photo-Optical Instrumentation Engineers (SPIE) Conference Series, VISTA data flow system: overview. pp 401–410

Fan X., Carilli C. L., Keating B., 2006, ARA&A, 44, 415

Fan X., et al., 2000, AJ, 119, 1

Fan X., et al., 2004, AJ, 128, 515

Fan X., et al., 2006, AJ, 132, 117

Fan X., Narayanan V. K., Lupton R. H., Strauss M. A., Knapp G. R., Becker R. H., White R. L., Pentericci L., et al., 2001, AJ, 122, 2833

Fan X., Strauss M. A., Schneider D. P., Becker R. H., White

Table B1. Adapted from Table 9 of Peth et al. (2011). CTIO/DECam, PanSTARRS/PS1, LSST Filter only values. From González-Fernández et al. (2018) $Z_{\rm AB} - Z_{\rm Vega} = 0.502$; $Y_{\rm AB} - Y_{\rm Vega} = 0.600$; $J_{\rm AB} - J_{\rm Vega} = 0.916$; $H_{\rm AB} - H_{\rm Vega} = 1.366$; $Ks_{\rm AB} - Ks_{\rm Vega} = 1.827$; and the CASU Vega to AB conversions v1.3:: Z,Y,J,H,Ks were: 0.524, 0.618, 0.937, 1.384, 1.839. So, Δ(vs. Gonzalez-Fernandez):: (11.2, 1.1, 5.4, 1.6, 0.1) millimags. Δ(vsCASU v1.3):: (-10.8, -16.9, -15.6, -16.4, -11.9) millimags.

Band	$\lambda_{\rm eff}$ Å	$\lambda_{\rm min}$ Å	$\lambda_{\rm max}$ Å	W$_{\rm eff}$ Å	AB - Vega	Transformations
$g_{\rm LSST}$	4730	3877	5665	1333	$g_{\rm LSST}$	$= g_{\rm AB} + 0.083$
$g_{\rm DECam}$	4734	3939	5528	1133	$g_{\rm DECam}$	$= g_{\rm AB} + 0.083$
$g_{\rm PS1}$	4776	3943	5593	1167	$g_{\rm PS1}$	$= g_{\rm AB} + 0.080$
$r_{\rm PS1}$	6130	5386	7036	1318	$r_{\rm PS1}$	$= r_{\rm AB} - 0.153$
$r_{\rm LSST}$	6139	5375	7055	1338	$r_{\rm LSST}$	$= r_{\rm AB} - 0.155$
$r_{\rm DECam}$	6345	5506	7238	1379	$r_{\rm DECam}$	$= r_{\rm AB} - 0.192$
$i_{\rm PS1}$	7485	6778	8304	1243	$i_{\rm PS1}$	$= i_{\rm AB} - 0.369$
$i_{\rm LSST}$	7487	6765	8325	1209	$i_{\rm LSST}$	$= i_{\rm AB} - 0.369$
$i_{\rm DECam}$	7750	6950	8646	1371	$i_{\rm DECam}$	$= i_{\rm AB} - 0.415$
$z_{\rm PS1}$	8658	8028	9346	966	$z_{\rm PS1}$	$= z_{\rm AB} - 0.508$
$z_{\rm LSST}$	8669	8035	9375	994	$z_{\rm LSST}$	$= z_{\rm AB} - 0.509$
$Z_{\rm VIRCAM}$	8762	8157	9400	978	$Z_{\rm VIRCAM}$	$= z_{\rm AB} - 0.513$
$Z_{\rm WFCAM}$	8802	8129	9457	926	$Z_{\rm WFCAM}$	$= z_{\rm AB} - 0.514$
$z_{\rm DECam}$	9216	8360	10166	1502	$z_{\rm DECam}$	$= z_{\rm AB} - 0.521$
$y_{\rm PS1}$	9603	9100	10838	615	$y_{\rm PS1}$	$= y_{\rm AB} - 0.541$
$y_{\rm LSST}$	9677	9089	10859	810	$y_{\rm LSST}$	$= y_{\rm AB} - 0.546$
$Y_{\rm DECam}$	9876	9355	10730	676	$Y_{\rm DECam}$	$= Y_{\rm AB} - 0.570$
$Y_{\rm WFCAM}$	10305	9790	10810	1020	$Y_{\rm WFCAM}$	$= Y_{AB} - 0.617$
$Y_{\rm VIRCAM}$	10184	9427	10977	905	$Y_{\rm VISTA}$	$= Y_{AB} - 0.601$
$J_{\rm VIRCAM}$	12464	11427	13759	1628	$J_{\rm VISTA}$	$= J_{AB} - 0.921$
$J_{\rm WFCAM}$	12483	11690	13280	1590	$J_{\rm WFCAM}$	$= J_{AB} - 0.919$
$W_{\rm Wircam}$	14514	13890	15166	1020	$W_{\rm Wircam}$	$= W_{AB} - 1.163$
$H_{\rm WFCAM}$	16313	14920	17840	2920	$H_{\rm WFCAM}$	$= H_{AB} - 1.379$
$H_{\rm VIRCAM}$	16310	14604	18422	2833	$H_{\rm VISTA}$	$= H_{AB} - 1.368$
$Ks_{\rm VIRCAM}$	21337	19333	23674	3055	$Ks_{\rm VISTA}$	$= Ks_{AB} - 1.83$
$K_{\rm WFCAM}$	22010	20290	23800	3510	$K_{\rm WFCAM}$	$= K_{AB} - 1.9$
WISE W1	33526	27541	38724	6626	W1	$= {\rm W1}_{\rm AB} - 2.699$
WISE W2	46028	39633	53414	10423	W2	$= {\rm W2}_{\rm AB} - 3.339$
WISE W3	115608	74430	172613	55056	W3	$= {\rm W3}_{\rm AB} - 5.174$
WISE W4	228172	195201	279107	41017	W4	$= {\rm W4}_{\rm AB} - 6.66$

R. L., Haiman Z., Gregg M., Pentericci L., et al. 2003, AJ, 125, 1649

Flaugher B., 2005, International Journal of Modern Physics A, 20, 3121

Flaugher B., et al., 2015, AJ, 150, 150

Flewelling H. A., et al., 2016, arXiv:1612.05243v2

Fukugita M., Ichikawa T., Gunn J. E., Doi M., Shimasaku K., Schneider D. P., 1996, AJ, 111, 1748

González-Fernández C., et al., 2018, MNRAS, 474, 5459

Goto T., 2006, MNRAS, 371, 769

Haardt F., Gorini V., Moschella U., Treves A., Colpi M., eds, 2016, Astrophysical Black Holes Vol. 905 of Lecture Notes in Physics, Berlin Springer Verlag

Hambly N. C., Collins R. S., Cross N. J. G., et al. 2008, MNRAS, 384, 637

Hambly N. C., et al., 2008, MNRAS, 384, 637

Hewett P. C., Warren S. J., Leggett S. K., Hodgkin S. T., 2006, MNRAS, 367, 454

Hickox R. C., Myers A. D., Greene J. E., Hainline K. N., Zakamska N. L., DiPompeo M. A., 2017, ApJ, 849, 53

Hill A. R., Gallagher S. C., Deo R. P., Peeters E., Richards G. T., 2014, MNRAS, 438, 2317

Ikeda H., Nagao T., Matsuoka K., Kawakatu N., Kajisawa M., Akiyama M., Miyaji T., Morokuma T., 2017, ApJ, 846, 57

Jiang L., et al., 2006, AJ, 132, 2127

Jiang L., et al., 2008, AJ, 135, 1057

Jiang L., et al., 2009, AJ, 138, 305

Jiang L., et al., 2010, Nat, 464, 380

Jiang L., McGreer I. D., Fan X., Bian F., Cai Z., Clément B., Wang R., Fan Z., 2015, AJ, 149, 188

Kaiser N., et al., 2002, in J. A. Tyson & S. Wolff ed., Society of Photo-Optical Instrumentation Engineers (SPIE) Vol. 4836, Pan-STARRS: A Large Synoptic Survey Telescope Array. pp 154–164

Kaiser N., et al., 2010, in Society of Photo-Optical Instrumentation Engineers (SPIE) Vol. 7733, The Pan-STARRS wide-field optical/NIR imaging survey. p. 0

Kashikawa N., Ishizaki Y., Willott C. J., Onoue M., Im M., Furu-

sawa H., Toshikawa J., Ishikawa S., Niino Y., Shimasaku K., Ouchi M., Hibon P., 2015, ApJ, 798, 28
Kim Y., et al., 2015, ApJ Lett., 813, L35
Koptelova E., Hwang C.-Y., Yu P.-C., Chen W.-P., Guo J.-K., 2017, Scientific Reports, 7, 41617
Kurk J. D., et al., 2007, ApJ, 669, 32
Kurk J. D., Walter F., Fan X., Jiang L., Jester S., Rix H.-W., Riechers D. A., 2009, ApJ, 702, 833
Lacy M., et al., 2004, ApJS, 154, 166
Latif M. A., Volonteri M., Wise J. H., 2018, arXiv:1801.07685v1
Lawrence A., 2016, in Mickaelian A., Lawrence A., Magakian T., eds, Astronomical Surveys and Big Data Vol. 505 of Astronomical Society of the Pacific Conference Series, Clues to the Structure of AGN Through Massive Variability Surveys. p. 107
Leipski C., et al., 2014, ApJ, 785, 154
Lupi A., Haardt F., Dotti M., Fiacconi D., Mayer L., Madau P., 2016, MNRAS, 456, 2993
Lupton R. H., Gunn J. E., Szalay A. S., 1999, AJ, 118, 1406
Madau P., Haardt F., Dotti M., 2014, ApJ Lett., 784, L38
Magnier E. A., et al., 2016a, arXiv:1612.05242v2
Magnier E. A., et al., 2016b, arXiv:1612.05244v2
Magnier E. A., et al., 2016c, arXiv:1612.05240v2
Mahabal A., Stern D., Bogosavljević M., Djorgovski S. G., Thompson D., 2005, ApJ Lett., 634, L9
Matsuoka Y., et al., 2016, ApJ, 828, 26
Matsuoka Y., et al., 2018a, PASJ, 70, S35
Matsuoka Y., et al., 2018b, arXiv:1803.01861v2
Mazzucchelli C., et al., 2017, ApJ, 849, 91
McGreer I. D., Becker R. H., Helfand D. J., White R. L., 2006, ApJ, 652, 157
McGreer I. D., et al., 2013, ApJ, 768, 105
Morganson E., et al., 2012, AJ, 143, 142
Mortlock D., 2016, in Mesinger A., ed., Understanding the Epoch of Cosmic Reionization: Challenges and Progress Vol. 423 of Astrophysics and Space Science Library, Quasars as Probes of Cosmological Reionization. p. 187
Mortlock D. J., et al., 2009, Astron. & Astrophys., 505, 97
Mortlock D. J., et al., 2011, Nat, 474, 616
Mullaney J. R., Alexander D. M., Fine S., Goulding A. D., Harrison C. M., Hickox R. C., 2013, MNRAS, 433, 622
Oke J. B., Gunn J. E., 1983, ApJ, 266, 713
Peth M. A., Ross N. P., Schneider D. P., 2011, AJ, 141, 105
Pezzulli E., Valiante R., Schneider R., 2016, MNRAS, 458, 3047
Pezzulli E., Volonteri M., Schneider R., Valiante R., 2017, MNRAS, 471, 589
Reed S. L., et al., 2015, MNRAS, 454, 3952
Reed S. L., et al., 2017, MNRAS, 468, 4702
Rees M. J., 1984, ARA&A, 22, 471
Richards G. T., et al., 2006, ApJS, 166, 470
Sawicki M., 2002, AJ, 124, 3050
Shanks T., et al., 2015, MNRAS, 451, 4238
Simcoe R. A., Sullivan P. W., Cooksey K. L., Kao M. M., Matejek M. S., Burgasser A. J., 2012, Nat, 492, 79
Stern D., et al., 2005, ApJ, 631, 163
Stern D., et al., 2007, ApJ, 663, 677
Stern D., et al., 2012, ApJ, 753, 30
Sun M., et al., 2015, ApJ, 802, 14
Takeo E., Inayoshi K., Ohsuga K., Takahashi H. R., Mineshige S., 2018, MNRAS, 476, 673
Tang J.-J., et al., 2017, MNRAS, 466, 4568
Taylor M., , 2011, TOPCAT: Tool for OPerations on Catalogues And Tables, Astrophysics Source Code Library
Taylor M. B., 2005, in Shopbell P., Britton M., Ebert R., eds, Astronomical Data Analysis Software and Systems XIV Vol. 347 of Astronomical Society of the Pacific Conference Series, TOPCAT & STIL: Starlink Table/VOTable Processing Software. p. 29
The Astropy Collaboration et al., 2018, ArXiv e-prints
Tielens A. G. G. M., 2008, ARA&A, 46, 289
Timlin J. D., Ross N. P., et al., 2016, ApJS, 225, 1
Valiante R., Schneider R., Graziani L., Zappacosta L., 2018, MNRAS, 474, 3825
Venemans B. P., et al., 2012, ApJ Lett., 751, L25
Venemans B. P., et al., 2013, ApJ, 779, 24
Venemans B. P., et al., 2015a, MNRAS, 453, 2259
Venemans B. P., et al., 2015b, ApJ Lett., 801, L11
Venemans B. P., McMahon R. G., Warren S. J., Gonzalez-Solares E. A., Hewett P. C., Mortlock D. J., Dye S., Sharp R. G., 2007, MNRAS, 376, L76
Venemans B. P., Walter F., Zschaechner L., Decarli R., De Rosa G., Findlay J. R., McMahon R. G., Sutherland W. J., 2016, ApJ, 816, 37
Volonteri M., 2010, A&ARv, 18, 279
Volonteri M., Silk J., Dubus G., 2015, ApJ, 804, 148
Wang F., et al., 2017, ApJ, 839, 27
Wang F., Wu X.-B., Fan X., Yang J., Yi W., Bian F., McGreer I. D., Yang Q., Ai Y., Dong X., Zuo W., Jiang L., Green R., Wang S., Cai Z., Wang R., Yue M., 2016, ApJ, 819, 24
Wang R., et al., 2008, ApJ, 687, 848
Wang R., et al., 2010, ApJ, 714, 699
Wang R., et al., 2011, ApJ Lett., 739, L34
Wang R., et al., 2013, ApJ, 773, 44
Wang R., et al., 2016, ApJ, 830, 53
Waters C. Z., et al., 2016, arXiv:1612.05245v4
Willott C. J., Albert L., Arzoumanian D., Bergeron J., Crampton D., Delorme P., Hutchings J. B., Omont A., Reylé C., Schade D., 2010, AJ, 140, 546
Willott C. J., Bergeron J., Omont A., 2015, ApJ, 801, 123
Willott C. J., et al., 2007, AJ, 134, 2435
Willott C. J., et al., 2009, AJ, 137, 3541
Willott C. J., et al., 2010, AJ, 139, 906
Willott C. J., Omont A., Bergeron J., 2013, ApJ, 770, 13
Wright E. L., Eisenhardt P. E., Fazio G. G., 1994, ArXiv Astrophysics e-prints
Wu X.-B., et al., 2015, Nat, 518, 512
Wyithe J. S. B., Loeb A., 2003, ApJ, 586, 693
Yan L., Sajina A., Fadda D., Choi P., Armus L., Helou G., Teplitz H., Frayer D., Surace J., 2007, ApJ, 658, 778
Yang G., et al., 2018, MNRAS, 475, 1887
Zeimann G. R., White R. L., Becker R. H., Hodge J. A., Stanford S. A., Richards G. T., 2011, ApJ, 736, 57